Supporting Information

Multistage transdermal nitric oxide delivery system for the efficient treatment of androgenic alopecia

*Hui Xing [a, b,1], Xinlin Jiang [a, b,1], Ziyi Zhao [b], Yuhui Yang [b], Zhen Wang [b], Yang Yi [b], Guodong Sun [a], Shixin Liu [a, *], Dong Ma [a, b *]*

H. Xing,

[a] Guangdong Provincial Key Laboratory of Spine and Spinal Cord Reconstruction, The Fifth Affiliated Hospital (Heyuan Shenhe People's Hospital), Jinan University, Heyuan 517000, China.

[b] Key Laboratory of Biomaterials of Guangdong Higher Education Institutes, Department of Biomedical Engineering, Jinan University, Guangzhou 510632, China.

X. Jiang

[a] Guangdong Provincial Key Laboratory of Spine and Spinal Cord Reconstruction, The Fifth Affiliated Hospital (Heyuan Shenhe People's Hospital), Jinan University, Heyuan 517000, China.

[b] Key Laboratory of Biomaterials of Guangdong Higher Education Institutes, Department of Biomedical Engineering, Jinan University, Guangzhou 510632, China.

Z. Zhao

[b] Key Laboratory of Biomaterials of Guangdong Higher Education Institutes, Department of Biomedical Engineering, Jinan University, Guangzhou 510632, China.

Y. Yang

[b] Key Laboratory of Biomaterials of Guangdong Higher Education Institutes, Department of Biomedical Engineering, Jinan University, Guangzhou 510632, China.

Z. Wang

[b] Key Laboratory of Biomaterials of Guangdong Higher Education Institutes, Department of Biomedical Engineering, Jinan University, Guangzhou 510632, China.

Y. Yi

[b] Key Laboratory of Biomaterials of Guangdong Higher Education Institutes, Department of Biomedical Engineering, Jinan University, Guangzhou 510632, China.

G. Sun

[a] Guangdong Provincial Key Laboratory of Spine and Spinal Cord Reconstruction, The Fifth Affiliated Hospital (Heyuan Shenhe People's Hospital), Jinan University, Heyuan 517000, China.

S. Liu

[a] Guangdong Provincial Key Laboratory of Spine and Spinal Cord Reconstruction, The Fifth Affiliated Hospital (Heyuan Shenhe People's Hospital), Jinan University, Heyuan 517000, China.

E-mail: liushixin@jnu.edu.cn

D. Ma

[a] Guangdong Provincial Key Laboratory of Spine and Spinal Cord Reconstruction, The Fifth Affiliated Hospital (Heyuan Shenhe People's Hospital), Jinan University, Heyuan 517000, China.

[b] Key Laboratory of Biomaterials of Guangdong Higher Education Institutes, Department of Biomedical Engineering, Jinan University, Guangzhou 510632, China.

E-mail: tmadong@jnu.edu.cn

*Corresponding authors.

Materials. Soy lecithin (CAS: 8030-76-0) and Tween 80 (CAS: 9005-65-6) were sourced from Shandong Tianchen Biotechnology (Shandong, China). Polyvinyl alcohol (PVA CAS: 9002-89-5), and glycerol (CAS: 56-81-5) were supplied by Shanghai Daishang Chemical (Shanghai, China). Cholesteryl chloroformate (Cho CAS: 7144-08-3) was acquired from Shandong Freda Biotechnology (Shandong, China). Sodium hyaluronate (CAS: 9067-32-7) was provided by Hengqin Perfect-Medical Laboratory Co. Ltd (Zhuhai, China). Minoxidil was obtained from Dafeixin. The Griess reagent kit, CCK-8 assay, and Calcein/PI kits were purchased from Beyotime Biotechnology (Shanghai, China). HDPCs were obtained from Meisen Cell Technology Co., Ltd. (Zhejiang, China). HUVECs were obtained from Procell Life Science&Technology Co., Ltd. (Wuhan, China).

Preparation of primary NO delivery carriers. The preparation process was refined and optimized drawing on insights from previous studies[1,2]. Initially, polyethyleneimine was dissolved in anhydrous dichloromethane under vigorous stirring in an ice bath. Under the catalysis of triethylamine, an anhydrous dichloromethane solution containing cholesterol chloroformate was added to the reaction system. Following a 7-hour reaction, the organic solvent was then removed using a rotary evaporator, and the resulting product was redissolved in a 0.1 M hydrochloric acid solution. The redissolved product was extracted twice with dichloromethane and washed multiple times with acetone. Finally, the white product Cho-PEI was obtained by vacuum drying. The Cho-PEI was further dissolved in anhydrous methanol, and sodium methoxide was added to create an alkaline environment. The mixture was then placed in a high-pressure NO reactor, maintained at 80 psi, and stirred for three days. After precipitation with acetone and vacuum drying, the ionic NO donor material Cho-PEI/NONOate was obtained. The preparation of HL/NONOate followed a previously established protocol[3]. Soy lecithin (3%, w/v) and Cho-PEI/NONOate (0.01%, w/v) were dissolved in an ethanol/chloroform mixture (30 mL, 1:1, v/v) until fully dissolved, followed by the addition of hyaluronic acid solution (0.05%, w/v). The mixture was processed by high-speed homogenization, rotary evaporation, and microfluidization to obtain an HL/NONOate suspension. The same procedure was followed to obtain HL, with Cho-

PEI replacing Cho-PEI/NONOate.

Characterization of primary NO delivery carriers. For nuclear magnetic resonance (NMR) spectroscopy, 2 mg each of carrier construction materials were dissolved in deuterated chloroform and transferred into clean NMR tubes. For FTIR spectroscopy, appropriate amounts of carrier construction materials were placed into a clean agate mortar, mixed, and ground with dry potassium bromide powder to form transparent pellets. These pellets were then analyzed using an FTIR spectrometer. The stability of HL and HL/NONOate was evaluated over a seven-day period using dynamic light scattering (DLS) with a Malvern laser particle size analyzer. This analysis focused on monitoring variations in particle size, zeta potential, and the polydispersity index (PDI). Spectral changes were determined by placing appropriate amounts of HL and HL/NONOate samples into clean UV cuvettes and measuring the spectra at room temperature using a UV-Vis spectrophotometer. Morphological changes were observed by adding appropriate amounts of HL and HL/NONOate solutions onto carbon film-coated copper grids, staining with phosphotungstic acid, drying, and analyzing using transmission electron microscopy (TEM).

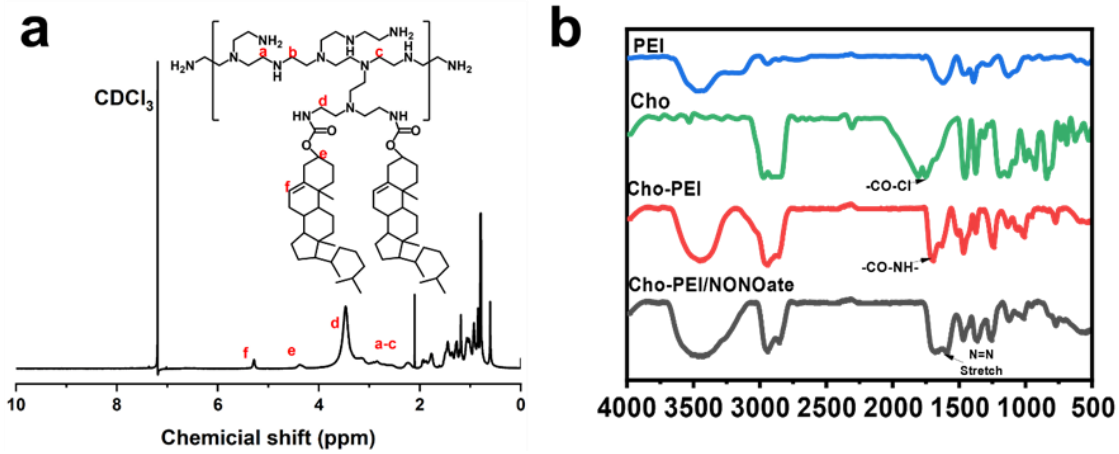

Figure. S1. (a) ^{1}H NMR spectra of Cho-PEI. (b) FT-IR spectra of PEI, Cho, Cho-PEI, and Cho-PEI/NONOate.

Analysis of NO loading and release. The NO content and release profile within HL/NONOate were analyzed using the Griess reagent assay[4]. To begin, 2 mg of NO donor materials was dissolved in 2 mL of citrate buffer (pH=4.0) and incubated at a constant temperature for 4 hours. Post-incubation, the solution underwent

centrifugation, after which the supernatant was collected and mixed with the Griess reagent. This mixture was then kept for 20 minutes before measuring absorbance at 540 nm. For the release study, 2 mL of HL/NONOate solution was placed in a dialysis bag with a molecular weight cutoff of 500 Da and immersed in a centrifuge tube containing 48 mL of PBS buffer at 37□. At predetermined intervals, 2 mL of the solution was withdrawn from the tube and replaced with an equal volume of PBS buffer. The withdrawn solution was treated with the Griess reagent for 20 minutes, followed by absorbance measurement at 540 nm.

Effect of NO on HDPCs proliferation. The impact of NO on the proliferation of HDPCs was assessed using the Cell Counting Kit-8 (CCK-8) assay. In brief, HDPCs were seeded in a 96-well plate and incubated at 37°C with 5% CO□ for one day to allow for cell attachment[5]. After cell attachment, HL/NONOate containing different concentrations of NO (1, 2, 10, 20, 40, 80, 200 μM) was added. Each condition was tested in triplicate. Following an additional 24-hour incubation period, the medium was removed, and the CCK-8 reagent was added to each well. The cells were then incubated for an additional hour, after which the absorbance was measured at 450 nm[6]. The proliferation assay for HUVECs was conducted using the same protocol.

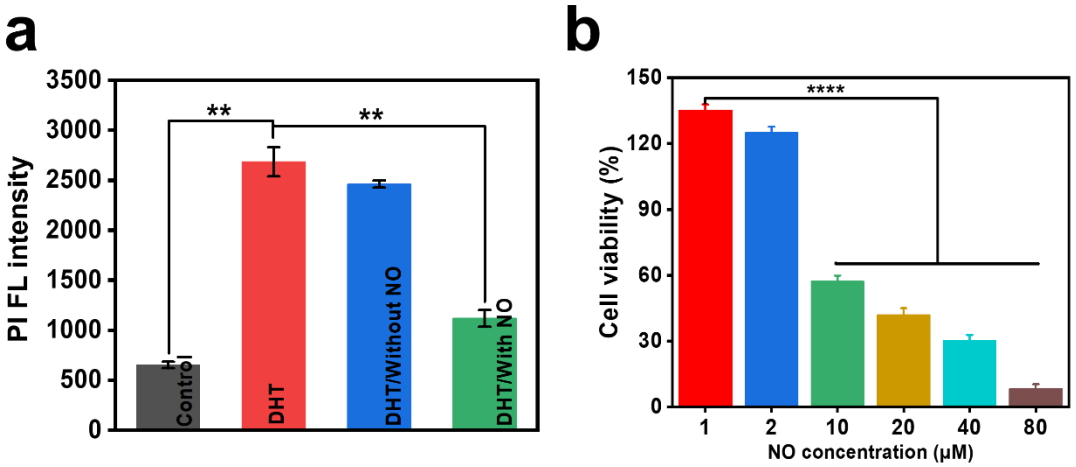

Figure. S2. (a) Quantitative analysis of PI fluorescence intensity in Figure 2e. (b) Proliferation rates of HUVECs after treatments with different concentrations of NO (1, 2, 10, 20, 40 and 80 μM, n=3). *$p < 0.05$, **$p < 0.01$, ***$p < 0.001$ and ****$p < 0.0001$.

NO effect on HDPCs migration experiment. To investigate the impact of NO on

HDPCs viability, a scratch assay was conducted to assess cell migration[7]. HDPCs were seeded in a 6-well plate and after one day of incubation, a scratch was made in the center of each well. The wells were then treated with HL/NONOate at varying NO concentrations (1, 2, 10, 20, 40 μM). Following 24 hours of co-incubation, the images of the scratch area were captured. The scratch width was quantified, and the migration area was calculated. The migration assay for HUVECs was performed using the same protocol.

NO protection against DHT-induced damage in HDPCs. A DHT-induced cell damage model was used, similar to previous studies[8]. HDPC cells were seeded in a 24-well plate and cultured overnight until the cells adhered to the plate. The old culture medium was discarded, and different materials (DHT, DHT+HL, DHT+HL/NONOate, NO concentration of 1 μM) were added and incubated for one day. Live/dead cell staining was performed using a Calcein/PI staining kit, and photographs were taken using an inverted fluorescence microscope[9].

RNA sequencing. HDPCs cells were seeded in a 6-well plate and cultured overnight until the cells adhered to the plate. The old culture medium was discarded, and different materials (DHT, DHT+HL, DHT+HL/NONOate, NO concentration of 1 μM) were added and incubated for three days. RNA was extracted using the Trizol reagent kit, followed by agarose gel electrophoresis and a nano-spectrophotometer for strict quality control of RNA samples. cDNA was synthesized using the Prime-Script™ RT reagent kit according to the manufacturer's recommendations. Gene expression was quantified by calculating the number of reads per million mapped reads per kilobase of transcript[10].

qRT-PCR analysis. Based on the RNA sequencing results, qRT-PCR was employed to validate the expression of GLI2, TNFRSF9, IL6, IL-17A, and CXCL5 in normal or DHT-damaged HDPCs[11]. HDPCs were seeded in 6-well plates and after two days of treatment with different media (DHT, DHT+HL, DHT+HL/NONOate with an NO concentration of 1 μM), the total RNA was extracted using Trizol reagent[12]. Reverse transcription was performed using the appropriate kit, following the manufacturer’s instructions. Finally, gene expression levels of GLI2, TNFRSF9, IL6, IL-17A, and CXCL5 were measured. The primer sequences used are listed in Table S1.

Table S1. Primer sequences used for qRT-PCR in this study.

Gene	Forward/Reverse	Primer (5' to 3')
GLI2	Forward	AGGGATGACTGTAAGCAGGAGG
	Reverse	TGGATGTGCTCGTTGTTGATG
CXCL5	Forward	TAATCTGCAAGTGTTCGCCATAG
	Reverse	TCAGTTTTCCTTGTTTCCACCG
IL-17A	Forward	CTGTCCCCATCCAGCAAGAG
	Reverse	AGGCCACATGGTGGACAATC
TNFRSF9	Forward	GCTTTGGGACATTTAACGATCAG
	Reverse	AGAACAGCAGGAAGAGCAACG
IL-6	Forward	CAATGAGGAGACTTGCCTGGTG
	Reverse	TGGCATTTGTGGTTGGGTCA

Synthesis of multistage delivery carriers. In brief, varying concentrations of PVA (10%, 15%, 20%, w/v), along with Tween 80 (0.5%, w/v) and glycerol (0.5%, w/v), were dissolved in 10 mL of purified water and heated with stirring at 95°C until completely dissolved. Subsequently, the mixture was allowed to reach room temperature before the produced HL/NONOate (10%, w/v) suspension was added. The mixture was then stirred for 30 minutes to produce different concentrations of PVA@HL/NONOate.

Characterization of multistage delivery carriers. The micro-pore distribution was observed using a biological microscope and a scanning electron microscope (SEM). The viscosity changes of the material with temperature were characterized using a rotational rheometer. The application flexibility of the material (adhesion, twisting, bending, stretching) was characterized using pig skin, and its flowability on the skin was simulated using a glass slide. Finally, the film-forming performance and time of the material on human skin were determined.

Study on NO release in multistage delivery carriers. NO release from

PVA@HL/NONOate based on the above experimental procedures. For the release study, 1 mL of PVA@HL/NONOate solution was placed in a dialysis bag with a molecular weight cutoff of 500 Da and immersed in a centrifuge tube containing 49 mL of PBS buffer at 37□. At predetermined intervals, 2 mL of the solution was withdrawn from the tube and replaced with an equal volume of PBS buffer. The withdrawn solution was treated with the Griess reagent for 20 minutes, followed by absorbance measurement at 540 nm.

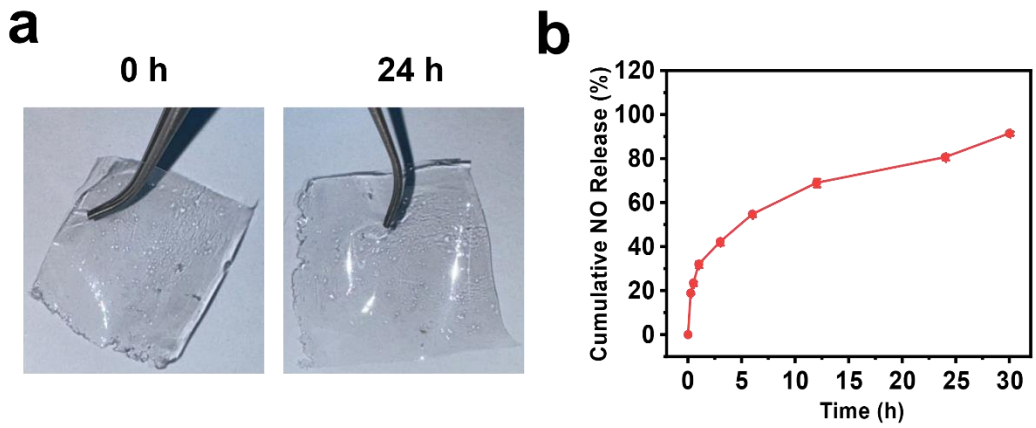

Figure. S3. (a) Morphological changes of the PVA@HL/NONOate film after 24 h. (b) NO release characteristics in the PVA@HL/NONOate (n=3).

Examination of the impact of multistage delivery carriers on NO penetration *in vitro*. The penetration of NO was assessed using a Franz diffusion cell, which simulates human skin penetration[13]. The diffusion cells were maintained at 37°C using a circulating water bath, and 12 mL of PBS was added to the receptor chamber with continuous stirring. A 2 cm^2 section of excised mouse dorsal skin was placed between the donor and receptor chambers. The donor chamber was filled with 2 mL of PVA@HL/NONOate or HL/NONOate suspensions at different PVA concentrations (10%, 15%, 20%), then sealed. Samples (200 μL) were collected from the receptor chamber at 2, 4, 8, and 12 hours, replaced with 200 μL of fresh PBS buffer, and mixed with Griess reagent. The absorbance at 540 nm was measured using a microplate reader and the NO concentration in the permeate solution was estimated[14].

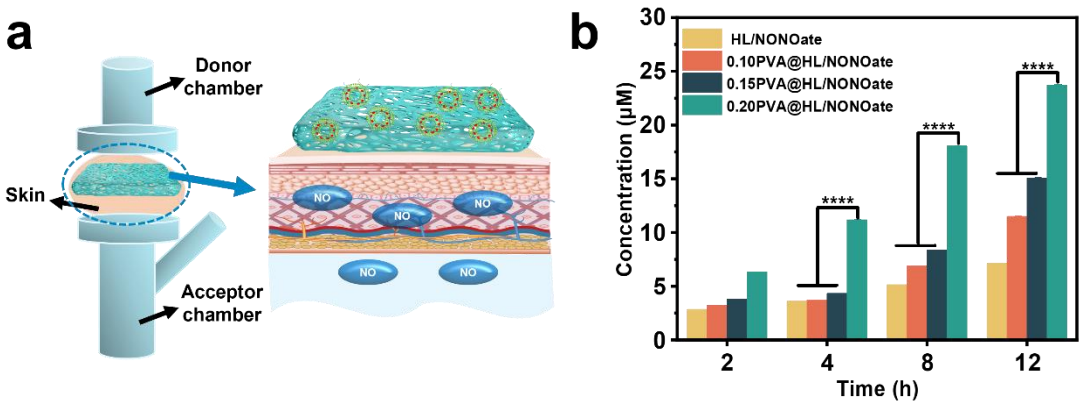

Figure. S4. (a) Diagram of the Franz diffusion cell used for the permeation enhancement study of PVA@HL/NONOate. (b) Permeation of NO through HL/NONOate and carriers of PVA@HL/NONOate at different concentrations over 12 hours (n=3). *$p < 0.05$, **$p < 0.01$, ***$p < 0.001$ and ****$p < 0.0001$.

Examination of the impact of multistage delivery carriers on NO penetration *in vivo*. The *in vivo* NO penetration was evaluated using live mice. Mice were first anesthetized and then shaved on their dorsal side. After 24 hours, 100 μL of PVA@HL/NONOate (PVA concentration of 20%) or HL/NONOate suspension was evenly applied to the shaved dorsal skin. After 1 hour, the dorsal skin tissue was excised, washed with PBS to remove residual materials, and dried. The tissue was then embedded in an optimal cutting temperature compound and fixed. The frozen skin tissue was sectioned into slices approximately 10 μm thick using a cryostat set at -20°C. The skin sections were subsequently stained with a Nitro-tyrosine immunohistochemistry kit and examined under a microscope to analyze the distribution of NO within the skin[15].

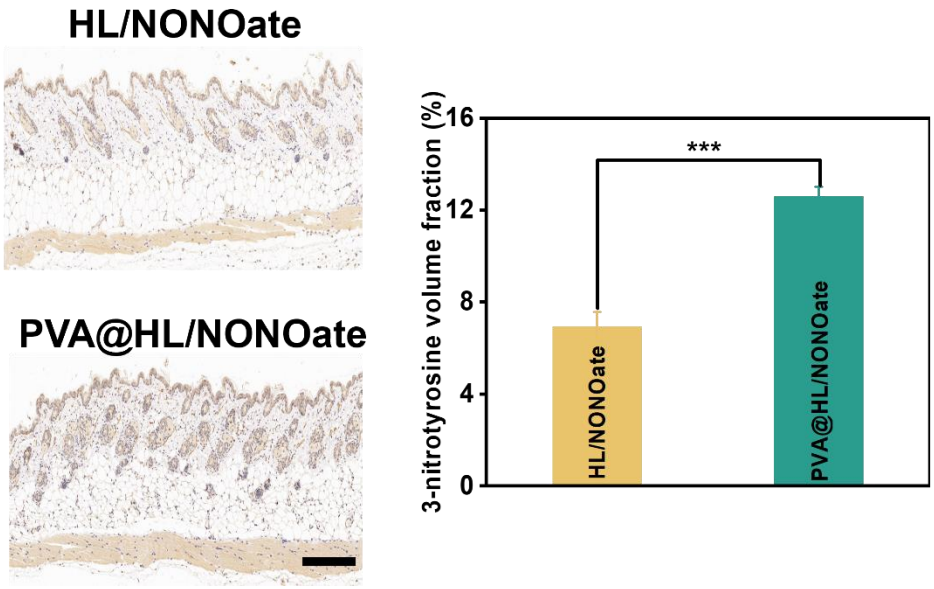

Figure. S5. Measurement of NO content in the live skin treated with HL/NONOate and 20% PVA@HL/NONOate. *$p < 0.05$, **$p < 0.01$, ***$p < 0.001$ and ****$p < 0.0001$.

Establishment and treatment of AGA mouse model. C57BL/6 female mice, each weighing approximately 20 g, were sourced from the Jinan University Center for Animal Experiment. The animal procedures were conducted following the National Research Council's Guide for the Care and Use of Laboratory Animals (2011) and were approved by the Animal Ethics Committee of Jinan University (Approval No.: IACUC-20230522-07). The AGA mouse model was established with modifications based on methods described in previous literature. Following hair removal using depilatory cream, the mice were subcutaneously injected with dihydrotestosterone (DHT) to induce an AGA model. DHT was administered at a dosage of 10 mg/kg per day, and this dosage was consistently maintained throughout the treatment period to sustain androgen levels in the mice[16]. Using female mice can avoid the effects of their own androgen DHT on hair loss as much as possible. The mice were assigned to six groups: Healthy control, AGA model, HL treatment, Minoxidil treatment, HL/NONOate treatment, and PVA@HL/NONOate treatment (PVA concentration of 20%), with four mice in each group. Topical treatments commenced on the first day following hair removal. The Healthy group was treated with saline, while the AGA group received only DHT injections. The treatments were applied for 21 days. Hair growth on the dorsal side was photographed on days 7, 12, 17, and 21. The dorsal skin was observed

with a dermatoscope to record hair growth, skin color changes, and the overall health of the mice.

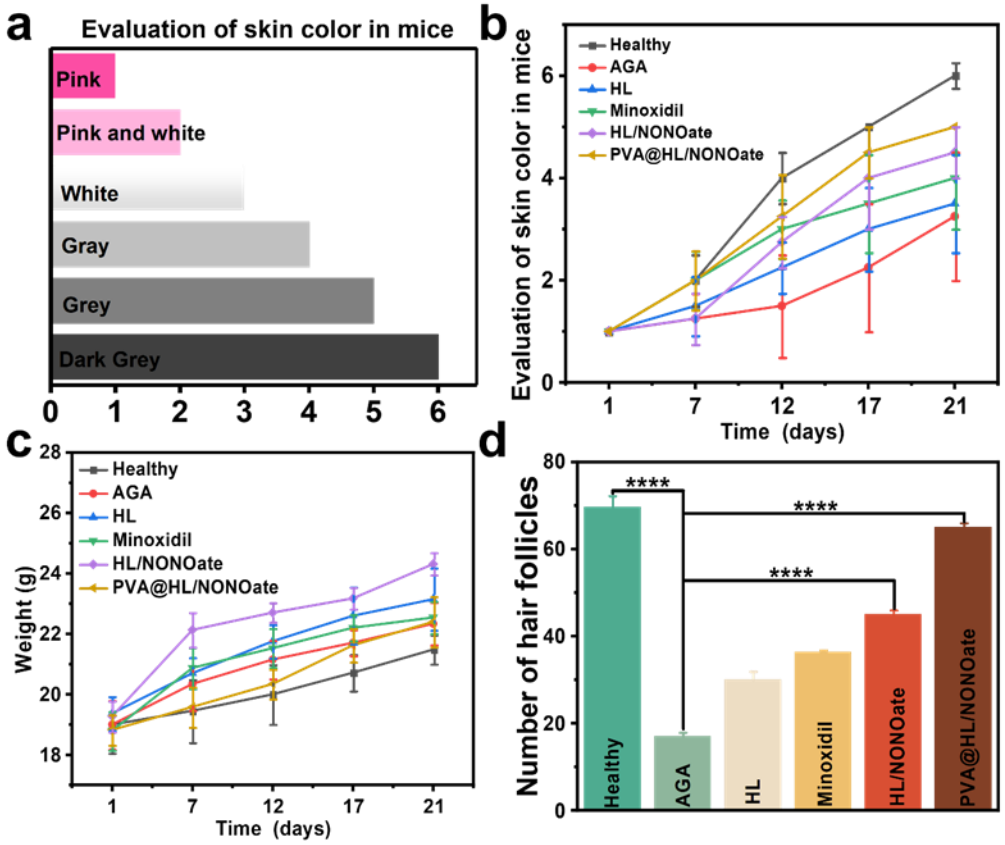

Figure. S6. (a) Mouse skin color scoring index. (b) Quantification based on the mouse skin color scores (n=4). (c) Body weight changes of the mice (n=4). (d) Number of hair follicles in the cross-sections of mouse skin (n=4). *$p < 0.05$, **$p < 0.01$, ***$p < 0.001$ and ****$p < 0.0001$.

Histological evaluation of mouse skin. The newly grown hair from the dorsal side of each mouse was collected, weighed, and examined microscopically. The dorsal skin tissue was then excised and fixed in a 4% paraformaldehyde solution. Following fixation, the tissue was embedded in paraffin, sectioned into thick slices, and stained with hematoxylin and eosin. The hair follicles in the skin tissue were observed under a light microscope, and the total number of hair follicles was quantified.

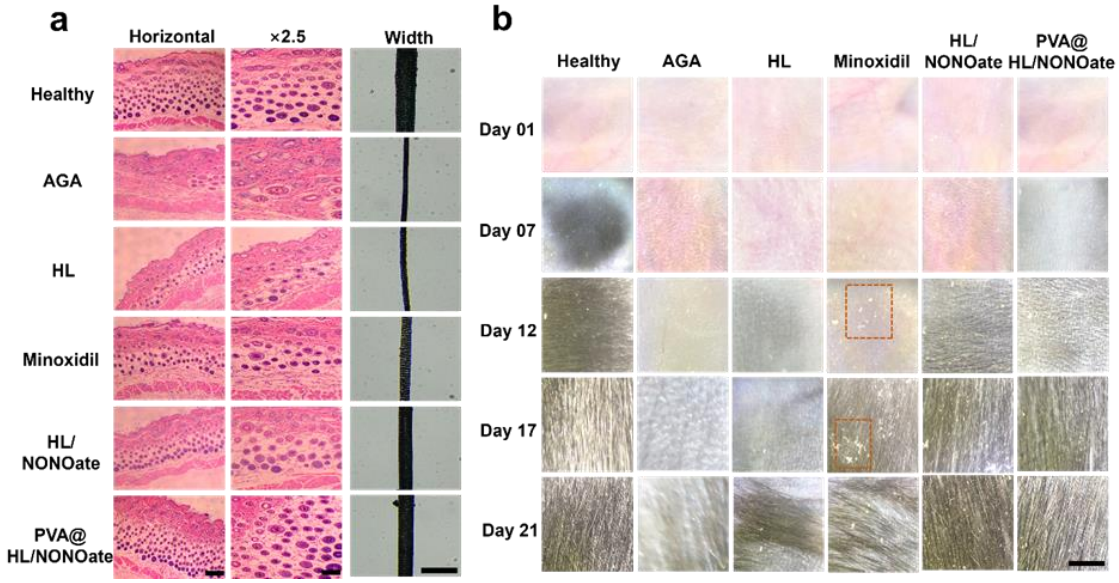

Figure. S7. (a) H&E staining of back skin and hair images under an optical microscope, the scale bars from left to right measure 100 μm, 50 μm, and 250 μm, respectively. (b) Dermatoscope images of hair growth in various groups of mice and skin safety analysis after continuous medication treatment.

Immunofluorescence staining. After the experiment, the dorsal skin tissue of each mouse was embedded in paraffin and sectioned. Antigen retrieval was performed, followed by blocking in mouse serum. Incubate sections with antibodies overnight at 4°C. Nuclei were counterstained with DAPI. The slides were then observed using a fluorescence microscope, and ImageJ was used to measure the fluorescence intensity.

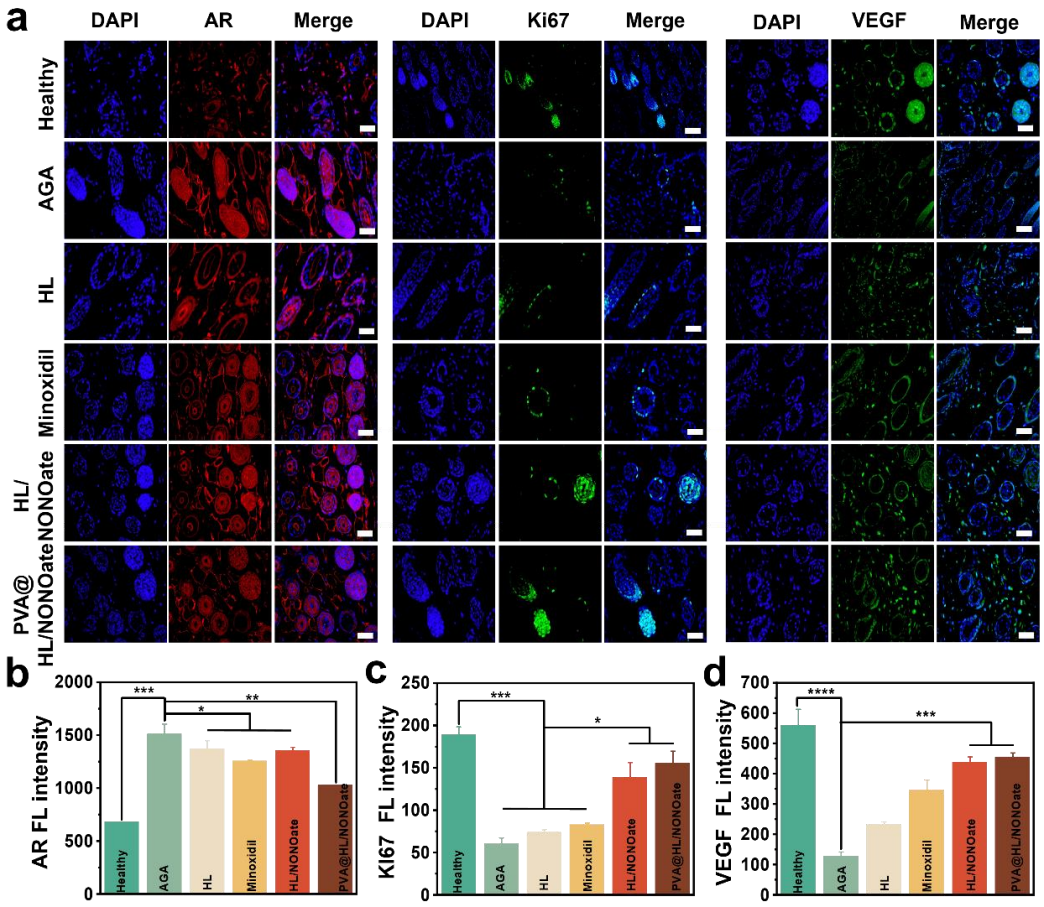

Figure. S8. (a) The fluorescence expression of AR, Ki67, and VEGF in the tissue microenvironment of mice, scale bar = 50 μm. (b) Quantitative evaluation of AR derived from (a). (c) Quantitative evaluation of Ki67 derived from (a). (d) Quantitative evaluation of VEGF derived from (a). **p < 0.05, **p < 0.01, ***p < 0.001 and ****p < 0.0001*.

ELISA analysis. Protein lysates were prepared from mouse skin tissue, dissolved in PBS, and subjected to ELISA to measure cytokine levels. The samples were diluted as determined by preliminary experiments. Subsequent steps were carried out according to the kit protocol. The color change was induced and then halted using the appropriate reagents, and the intensity of the color, which corresponds to the concentration of IL-6 and TGF-β1 in the samples, was measured at 450 nm[17].

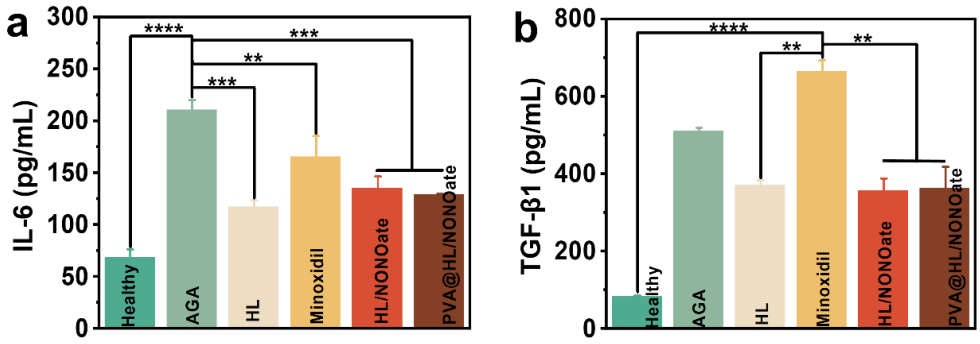

Figure. S9. (a) The content of IL-6 in skin tissue (n=4). (b) The content of TGF-β1 in skin tissue (n=4). *$p < 0.05$, **$p < 0.01$, ***$p < 0.001$ and ****$p < 0.0001$.

Skin toxicity test. To compare the skin side effects of Minoxidil, a commercially available drug, the toxicity of the materials to the skin was evaluated after continuous application on the back of mice for 12 days. Skin conditions such as peeling, scabbing, and edema were recorded using a dermatoscope.

***In vivo* toxicity.** At the end of the treatment period, blood samples were collected from each mouse, and serum was obtained via centrifugation. Liver and kidney function, along with other relevant biochemical parameters, were analyzed. The major organs were excised and then fixed in tissue fixative solution for subsequent histological analysis.

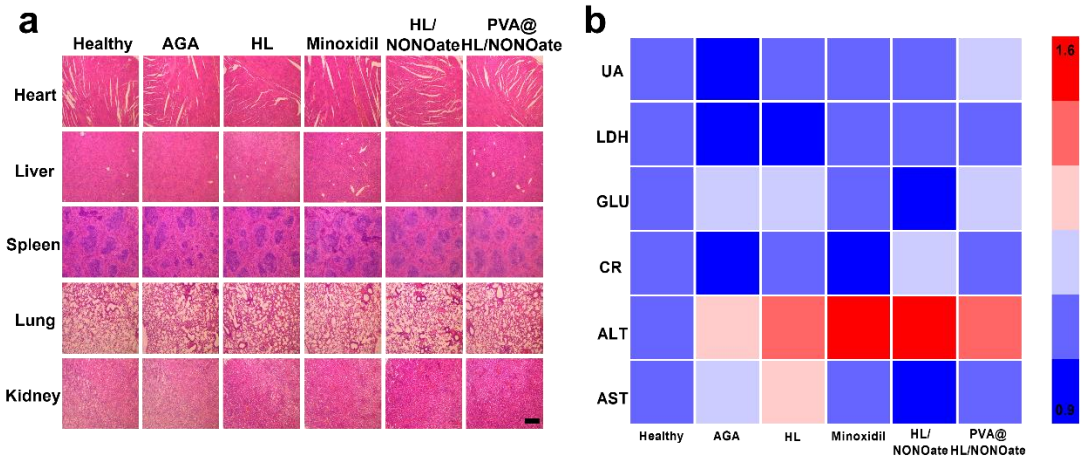

Figure. S10. (a) H&E staining pictures of major organs in mice, scale bar = 100 μm. (b) Biochemical analysis of mice serum after treatment with different materials, the maximum value in the figure is 1.6 times, which is in line with the normal content range (n=4).

Hemocompatibility Assay. 50 μL of a red blood cell suspension was added to 1 mL of

PVA@HL/NONOate solutions at varying concentrations. Pure water and PBS (pH = 7.4) were used as the positive and negative controls, respectively. After incubating at room temperature for 24 h, the mixtures were centrifuged at 1000 rmp for 5 minutes. The supernatant was collected and transferred to a 96-well plate, and the absorbance at 540 nm was measured. The hemolysis rate was calculated using the following formula:

$$\text{Hemolysis (\%)} = \frac{\text{A-C}}{\text{B-C}} * 100\%$$

where A, B, and C represent the absorbance of the PVA@HL/NONOate solution, positive control, and negative control, respectively.

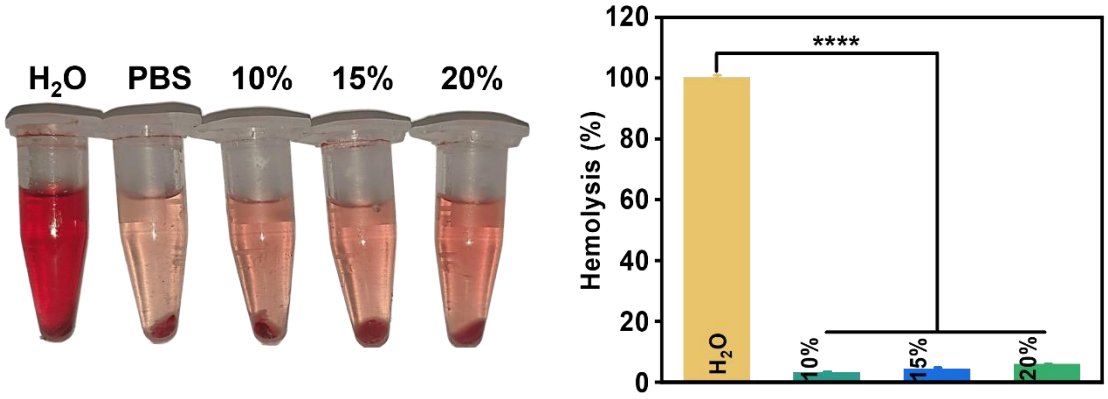

Figure. S11. Determination of hemolysis rate of PVA@HL/NONOate at different concentrations. *$p < 0.05$, **$p < 0.01$, ***$p < 0.001$ and ****$p < 0.0001$.

Statistical analysis. All experiments were performed in triplicate or more. All data are expressed as the mean ± standard deviation. Statistical differences among experimental groups were assessed using One-way ANOVA in GraphPad software. Significance levels were determined by P values, with thresholds set at *$P < 0.05$; **$P < 0.01$; ***$P < 0.001$; ****$P < 0.0001$.

AGA Treatment Perspectives. With advancements in technology, various treatment strategies for AGA have emerged over time. In this study, a multistage NO transdermal delivery system demonstrated promising results in treating AGA in mice. Here, we discuss different therapeutic approaches for AGA to gain further insights. Minoxidil and Finasteride, both FDA-approved drugs for hair loss treatment, are widely used[18]. However, Minoxidil formulations, which often use ethanol and propylene glycol as solvents, can cause scalp dryness, irritation, and itching. Finasteride, due to its hormonal mechanism of action, carries potential side effects such as sexual dysfunction

and gynecomastia. To mitigate these adverse effects, microneedle technology has also been introduced into AGA treatment[19]. When combined with these drugs, microneedles significantly reduce side effects and improve AGA outcomes, effectively overcoming the limitations of monotherapy. NO therapy provides a new approach for future combination treatments, offering hope for enhanced AGA treatment outcomes.

■REFERENCES

1. Li, G.; Lv, K.; Cheng, Q.; Xing, H.; Xue, W.; Zhang, W.; Lin, Q.; Ma, D., Enhanced Bacterial□Infected Wound Healing by Nitric Oxide□Releasing Topological Supramolecular Nanocarriers with Self□Optimized Cooperative Multi□Point Anchoring. *Adv Sci.* **2023**, *10*, 2206959.

2.Xing, H.; Peng, H.; Yang, Y.; Lv, K.; Zhou, S.; Pan, X.; Wang, J.; Hu, Y.; Li, G.; Ma, D., Nitric oxide synergizes minoxidil delivered by transdermal hyaluronic acid liposomes for multimodal androgenetic-alopecia therapy. *Bioact Mater.* **2024**, *32*, 190-205.

3. Dymek, M.; Sikora, E., Liposomes as biocompatible and smart delivery systems–The current state. *Adv Colloid Interface Sci.* **2022**, 102757.

4. Yu, S.; Li, G.; Liu, R.; Ma, D.; Xue, W., Dendritic Fe3O4@poly (dopamine)@ PAMAM nanocomposite as controllable NO□releasing material: a synergistic photothermal and NO antibacterial study. *Adv Funct Mater.* **2018**, *28*, 1707440.

5. Zhang, Z.; Li, W.; Chang, D.; Wei, Z.; Wang, E.; Yu, J.; Xu, Y.; Que, Y.; Chen, Y.; Fan, C., A combination therapy for androgenic alopecia based on quercetin and zinc/copper dual-doped mesoporous silica nanocomposite microneedle patch. *Bioact Mater.* **2023**, *24*, 81-95.

6. Zhang, Z.; Xu, R.; Wang, Z.; Dong, M.; Cui, B.; Chen, M., Visible-light neural stimulation on graphitic-carbon nitride/graphene photocatalytic fibers. *ACS Appl Mater Interfaces.* **2017**, *9*, 34736-34743.

7. Liang, C.-C.; Park, A. Y.; Guan, J.-L., *In vitro* scratch assay: a convenient and inexpensive method for analysis of cell migration *in vitro*. *Nat Protoc.* **2007**, *2*, 329-333.

8. Kang, J.-I.; Kim, S.-C.; Kim, M.-K.; Boo, H.-J.; Kim, E.-J.; Im, G.-J.; Kim, Y. H.; Hyun, J.-W.; Kang, J.-H.; Koh, Y.-S., Effects of dihydrotestosterone on rat dermal papilla cells *in vitro*. *Eur J Pharmacol.* **2015**, *757*, 74-83.

9. Xu, X.; Chen, Y.; Gui, J.; Liu, P.; Huang, Y.; Shao, B.; Ping, Y.; Li, B., A biomimetic nanodrug self-assembled from small molecules for enhanced ferroptosis therapy. *Biomater Sci.* **2022**, *10*, 770-780.

10. Ozsolak, F.; Milos, P. M., RNA sequencing: advances, challenges and opportunities. *Nat Rev Genet.* **2011**, *12*, 87-98.

11. Jozefczuk, J.; Adjaye, J., Quantitative real-time PCR-based analysis of gene expression. In *Methods in enzymology*, Elsevier: 2011; Vol. 500, pp 99-109.

12. Kim, Y.; Ryu, Y. C.; Min, H. S.; Yang, H.; Nam, J.; Lee, C.; Um, D. J.; Kim, M.; Atzei, P.; Francisco, R. d. B., Dual□Mode Vasodilator M119 Delivery to Hair Follicle via Dissolving Microneedle for Advanced Alopecia Treatment. *Adv Ther.* **2022**, *5*, 2200052.

13. Zhang, H.; Pan, D.; Dong, Y.; Su, W.; Su, H.; Wei, X.; Yang, C.; Jing, L.; Tang, X.; Li, X., Transdermal permeation effect of collagen hydrolysates of deer sinew on mouse skin, ex vitro, and antioxidant activity, increased type I collagen secretion of percutaneous proteins in NIH/3T3 cells. *J Cosmet Dermatol.* **2020**, *19*, 519-528.

14. Liu, S.; Cai, X.; Xue, W.; Ma, D.; Zhang, W., Chitosan derivatives co-delivering nitric oxide and methicillin for the effective therapy to the methicillin-resistant S. aureus infection. *Carbohydr Polym.* **2020**, *234*, 115928.

15. Zhou, S.; Wu, C.; Shen, P.; Zhou, L.; Wang, W.; Lv, K.; Wei, C.; Li, G.; Ma, D.; Xue, W., Tumor microenvironment-responsive multifunctional nanoplatform with selective toxicity for MRI-guided photothermal/photodynamic/nitric oxide combined cancer therapy. *Chem Eng J.* **2024**, *481*, 148618.

16. Zhang, X.; Li, S.; Dong, Y.; Rong, H.; Zhao, J.; Hu, H., A multifunctional cholesterol-free liposomal platform based on protopanaxadiol for alopecia therapy. *Nano Res.* **2022**, *15*, 9498-9510.

17. Chang, H.-P.; Kim, S. J.; Shah, D. K., Whole-body pharmacokinetics of antibody in mice determined using enzyme-linked immunosorbent assay and derivation of tissue

interstitial concentrations. *J Pharm Sci.* **2021**, *110*, 446-457.

18. Gupta, A. K.; Talukder, M.; Williams, G., Comparison of oral minoxidil, finasteride, and dutasteride for treating androgenetic alopecia. *J Dermatolog Treat.* **2022**, *33*, 2946-2962.

19. Ocampo□Garza, S. S.; Fabbrocini, G.; Ocampo□Candiani, J.; Cinelli, E.; Villani, A., Micro needling: A novel therapeutic approach for androgenetic alopecia, A Review of Literature. *Dermatol Ther.* **2020**, *33*, e14267.